NATIONAL ADVISORY COMMITTEE FOR AERONAUTICS

TECHNICAL NOTE 2228

EFFECTS OF MODIFICATIONS TO THE LEADING-EDGE REGION ON THE STALLING CHARACTERISTICS OF THE NACA 63_1-012 AIRFOIL SECTION

By John A. Kelly

Ames Aeronautical Laboratory
Moffett Field, Calif.

Washington
November 1950

NATIONAL ADVISORY COMMITTEE FOR AERONAUTICS

TECHNICAL NOTE 2228

EFFECTS OF MODIFICATIONS TO THE LEADING-EDGE REGION ON THE STALLING CHARACTERISTICS OF THE NACA 63_1-012 AIRFOIL SECTION

By John A. Kelly

SUMMARY

A wind-tunnel investigation of a series of modifications to the leading-edge region of the NACA 63_1-012 airfoil section was conducted to determine the possibilities of delaying the flow separation that occurs near the leading edge of the basic section and of improving the stalling characteristics thereby.

Increasing the leading-edge radius or adding thickness to the lower surface near the leading edge did not improve the stalling characteristics and resulted in only small increases in the maximum lift coefficient. Two cambered modifications were effective enough in delaying the leading-edge separation to permit turbulent separation to begin and extend over a portion of the airfoil near the trailing edge, thus causing a rounding of the lift-curve peak favorable to the stalling characteristics. Substantial increases in the maximum lift coefficient were also realized from the cambered modifications.

The movable-type modifications were three leading-edge flaps having different leading-edge radii, one of which conformed to that for the basic airfoil section. Deflection of the leading-edge flap for the basic section proved to be effective in increasing the maximum lift coefficient, but failed to improve the stalling characteristics. The effect of increasing the leading-edge radius of the flap was found to be negligible.

INTRODUCTION

The search for optimum airfoil sections for high-speed applications has focused attention on sections that are thinner than those in common usage because of their superior aerodynamic properties at high speed. However, these thinner sections are handicapped by their relatively low maximum lift coefficients and usually poor stalling characteristics. These deficiencies are the result of the mechanism of the stall of thin

sections. The flow separates from the leading edge prior to the separation of turbulent flow at the trailing edge of the airfoil. The abruptness of the flow separation is dependent on the individual airfoil section, and is usually severe for airfoils in the thickness ratio range from 10- to 12-percent chord.

Various methods of improving both the maximum lift and the stalling characteristics of thin sections have been more or less successful. Flaps at both the leading and the trailing edges are effective in increasing maximum lift, but relatively ineffective in alleviating the abruptness of the stall. Boundary-layer control by suction through a slot or porous surface near the leading edge has both increased the maximum lift and reduced the abruptness of the stall. These methods, however, add both complexity and weight to any practical application and are not failure proof in their operation.

In an attempt to provide a simpler means of improving stall characteristics, an investigation was undertaken to determine the effectiveness of alterations to the leading-edge region of an NACA 631-012 airfoil section. This section was chosen because a previous investigation (reference 1) had demonstrated that its stall was the result of an abrupt and complete separation of flow from the leading edge. The leading-edge alterations tested were of two general types. The first consisted of alterations to the first 15 percent of the profile, and the second, of alterations to the contour of a leading-edge flap hinged at the 15-percent-chord station on the lower surface.

The tests were conducted in the Ames 7- by 10-foot wind tunnel No. 1, and the results include force and pressure-distribution measurements.

SYMBOLS

A summary of the definitions of symbols used in this report is as follows:

c airfoil chord, feet

c_d drag coefficient[1] $\left(\frac{D}{q_o c}\right)$

c_l section lift coefficient $\left(\frac{L}{q_o c}\right)$

[1]The drag force measured by the wind-tunnel balance is a sum of the drag of the model and the skin-friction drag of the circular end plates attached to the model.

c_m section pitching-moment coefficient referred to quarter chord $\left(\frac{M}{q_o c^2}\right)$

D drag per unit span, pounds per foot[1]

L lift per unit span, pounds per foot

M pitching moment per unit span, pound-feet per foot

p_l local static pressure, pounds per square foot

p_o free-stream static pressure, pounds per square foot

P pressure coefficient $\left(\frac{p_l - p_o}{q_o}\right)$

q_o free-stream dynamic pressure $\left(\frac{1}{2}\rho_o V_o^2\right)$, pounds per square foot

V_o free-stream velocity, feet per second

x distance from basic airfoil leading edge measured parallel to chord line, feet

y distance measured normal to basic airfoil chord line, feet

α_o section angle of attack, degrees

δ leading-edge-flap deflection angle, degrees

ρ_o free-stream mass density, slugs per cubic foot

MODEL AND APPARATUS

The basic model used in this investigation had an NACA 63_1-012 airfoil section with a constant chord of 4 feet and spanned the 7-foot dimension of the wind-tunnel test section. The first 15 percent of the model chord was removable to accommodate the various leading-edge modifications (fig. 1(a)).

The model which conformed entirely to the NACA 63_1-012 coordinates will hereafter be referred to as the basic airfoil in this report. The modifications to the model were confined to the first 15 percent of the airfoil chord in all cases. Coordinates for the basic airfoil section and the various leading-edge modifications are presented in tables I and II, respectively.

The leading-edge modifications are derived as follows:

Modification 1 (1.5-percent-chord leading-edge radius).- The salient features of the development of modification 1 are shown in figure 1(b).

---

[1]See footnote 1, page 2.

A circle with a radius equal to 1.5 percent of the airfoil chord and having its center on the chord line was made tangent to the leading edge of the basic airfoil. The slope of the circle at $x/c = 0.0025$ was determined; and, together with the slope of the basic airfoil section at the 15-percent-chord station and an intermediate control point taken at $x/c = 0.025$, a second-degree equation for the new contour was developed (reference 2). The control point was arbitrarily located at the 2.5-percent-chord station to give nearly equal increases in thickness between the basic airfoil section and modification 1, and between modification 1 and modification 2.

Modification 2 (2-percent-chord leading-edge radius).- This modification was derived in the same manner as modification 1 except that a leading-edge radius of 2-percent chord was used.

Modification 3 (15-percent-chord thickness distribution).- The upper surface of this modification remained the same as that of the basic airfoil section; whereas the lower surface was altered by adding thickness such that the sum of the absolute values of the ordinates for the upper and lower surfaces was equal to the sum of the absolute values of the upper- and lower-surface ordinates for the NACA 63_2-015 airfoil section for corresponding chordwise stations (fig. 1(c)). This procedure was followed for the first 5 percent of the chord, whereupon the enlarged lower surface was arbitrarily faired back to the basic airfoil section at $x/c = 0.15$.

Modification 4 (18-percent-chord thickness distribution).- The derivation of this modification was identical to modification 3 except that an NACA 63_3-018 thickness distribution was provided for the first 5 percent of the chord (fig. 1(c)).

Modification 5 (2-percent-chord leading-edge radius plus circular-arc camber line forward of the 12.5-percent-chord point).- This modification was a combination of a circular-arc camber line forward of the 12.5-percent-chord point and modification 2. The circular-arc camber line was tangent to the chord line of the basic airfoil section at $x/c = 0.125$ and passed through the point $x/c = 0$, $y/c = -0.02$ (fig. 1(d)). The ordinates for modification 2 were then laid out normal to the camber line in accordance with the practice described in reference 3.

Modification 6 (offset 3.5-percent-chord leading-edge radius).- This modification was derived by constructing a circle with a radius of 3.5-percent chord tangent to the upper-surface contour of the basic airfoil section at $x/c = 0.0025$. The lower surface was faired from the basic airfoil at $x/c = 0.15$ tangent to the leading-edge circle at $x/c = 0.025$ (fig. 1(e)).

Leading-edge flaps.- Three leading-edge-flap arrangements were designed by hinging (1) the leading-edge region of the basic airfoil section, (2) the leading edge of modification 1, and (3) the leading edge of modification 2 about their lower surfaces at $x/c = 0.15$. (Only the

leading-edge flap for the basic airfoil section is shown in fig. 1(f).) A circular-arc block served as a fairing on the upper surface between the trailing edge of the flap and the 15-percent-chord station.

A row of static-pressure orifices was installed flush with the surface at the midspan section for all model arrangements except modifications 3 and 4.

TESTS

All tests were made with a dynamic pressure of 45 pounds per square foot, a Mach number of 0.177, and a Reynolds number, based on the 4-foot-chord dimension, of 4.92 million. The force data have been corrected for the constraint of the tunnel walls by the method of reference 4. Circular end plates, forming part of the tunnel floor and ceiling, were attached to the model. Measurements of drag of the model include the unknown tare drag of these circular end plates and are presented only as a means of comparison of incremental changes due to the various leading-edge modifications and not as an indication of the absolute values of the drag.

Considerable difficulty was encountered in obtaining data beyond the stall for some configurations due to violent buffeting and shaking of the model. Pressure distributions, measured by means of multiple-tube manometers, were recorded photographically. Flow patterns about each of the modifications were observed from indications of tufts spaced symmetrically about the midspan section over the entire upper surface of the model.

RESULTS AND DISCUSSION

Effect of Leading-Edge Modifications

Stalling characteristics.- A comparison of the stalling characteristics of the model with the various modifications may best be discussed by referring to figure 2. With modification 1 or 2, the stalling characteristics were nearly identical to those of the basic airfoil in that the peaks of the lift curves are sharp and there is little or no tendency for the curves to round over near maximum lift. The lift curves for modifications 3 and 4 are slightly more rounded immediately preceding $c_{l_{max}}$ than those previously mentioned, but tuft observations indicated that the flow was not separated over the trailing-edge region for any of these four modifications. Therefore, the additional rounding of the lift curves in the cases of modifications 3 and 4 can be attributed only to a thicker boundary layer over the rear portion of these models. However, the large and sudden loss in lift following maximum lift, characteristic of the basic airfoil section, also was observed for modifications 1, 2, 3, and 4. This type of stall is

generally a result of a failure of the separated boundary layer near the leading edge to reattach to the upper surface of the airfoil.

Previous investigations have shown that a small, localized region of separated flow is discernible on the upper surface near the leading edge of the NACA 63_1-012 for moderate angles of attack. This region - the so-called "bubble" of separated flow - moves forward along the surface as the angle of attack is increased. In reference 5 it was stated that the size of the region decreases with increasing Reynolds number. As the bubble moves forward along the surface of the airfoil it is subjected to increased local velocity which reduces its chordwise extent, but the increased curvature of the surface for the more forward location makes it more difficult for the separated flow to reattach to the surface. The limiting condition occurs when the effect of curvature overcomes the effect of increased velocity and the flow is no longer able to reattach to the surface. The amount of lift that is lost when the angle of attack for maximum lift has been exceeded depends on the extent of turbulent separation over the rear portion of the airfoil at the time of leading-edge separation.

With modification 5 or 6 some improvement in the stalling characteristics was obtained, as indicated by the slight rounding near the lift-curve peaks. This rounding is a result of separation of flow which occurred initially near the trailing edge of these airfoils. The complete stall of the airfoil, however, was probably the result of the failure of the separated flow near the leading edge to reattach to the surface of the model, thus providing the abrupt loss in lift once the maximum value was attained.

Maximum lift.- The effect of the leading-edge modifications was to increase the maximum lift in all cases (fig. 2). Modifications 1 and 3, although they differed radically in contour near the leading edge, had approximately the same leading-edge radius (1.5-percent chord), and the increases in maximum lift coefficient over that for the basic airfoil were 0.05 and 0.06, respectively. Modifications 2 and 4 likewise had dissimilar profiles near the leading edge but had approximately the same leading-edge radius (2-percent chord), and the increase in maximum lift coefficient over that for the basic airfoil was 0.14 for both modifications. Modification 5 increased $c_{l_{max}}$ 0.29 over that for the basic airfoil and 0.15 over that for modification 2, the uncambered counterpart of modification 5. The greatest increase in $c_{l_{max}}$ was obtained with modification 6 and amounted to 0.35 over that for the basic airfoil.

These results are summarized in the following table:

Airfoil section	$c_{l_{max}}$	Increase in $c_{l_{max}}$ over basic airfoil
Basic	1.36	-
Modification 1	1.41	0.05
Do. 2	1.50	.14
Do. 3	1.42	.06
Do. 4	1.50	.14
Do. 5	1.65	.29
Do. 6	1.71	.35

Drag.- The drag characteristics for the basic airfoil and the six modifications are presented in figure 3. In all cases for lift coefficients above 0.8, the drag coefficients of the modifications are less than those of the basic airfoil section. Even in the low-drag range for the basic airfoil section, the maximum increase in the drag coefficient for any of the modifications investigated, in this case modification 6, was on the order of 0.002.

Pitching moment.- Only when the modification incorporated a form of camber were the zero-lift pitching moments for the model changed from those of the basic airfoil (fig. 4). Even then the additional negative moment, prevalent at the low lift coefficients, tended to disappear as the values of the lift coefficient approached their maximum.

Pressure distribution.- Pressure distributions for the basic airfoil and the various modifications for approximately equal values of lift coefficient are presented in figure 5. Increasing the leading-edge radius without the inclusion of camber (modifications 1 and 2) had the effect of reducing and rounding the negative pressure peak and reducing the rate of pressure rise. The inclusion of camber (modifications 5 and 6) served to decrease further the peak and the adverse pressure gradient. These changes in the pressure distribution would delay the forward progression of the bubble of separated flow with increasing angle of attack and probably account for the greater maximum lift coefficients obtained with these modifications. In the case of modifications 1 and 2, the delay in forward progression of the bubble was slight and not sufficient to permit turbulent separation to start at the trailing edge. Progression of the localized flow separation toward the leading edge, however, was sufficiently delayed in the case of modifications 5 and 6 so that turbulent separation was permitted to start at the trailing edge. Tuft observations confirmed the onset of separation from the trailing-edge region and also indicated a steady forward progression of the turbulent separation point with increasing angle of attack. The region of nearly constant pressure coefficients in figure 6 suggests this area of turbulent-flow separation extended forward to approximately the 75-percent-chord station before $c_{l_{max}}$ was reached.

Effect of Leading-Edge Flap

Tests with the leading-edge-flap arrangements indicated only small effects due to changes in leading-edge radius; therefore, only data from tests of the model with the flap having the basic airfoil section are presented.

Stalling characteristics.- Deflecting the leading-edge flap proved to be only slightly effective in improving the stalling characteristics of the basic airfoil section. Improvement in stalling characteristics occurred for deflections of the leading-edge flap only in the range between 15° and 30° for which a slight rounding of the lift-curve peaks (fig. 7) was evident. In this range of flap deflections, tufts indicated that separation of the boundary layer over the trailing-edge portion of the airfoil occurred initially at an angle of attack several degrees below that for $c_{l_{max}}$. However, the stall associated with $c_{l_{max}}$ for all angles of deflection of the leading-edge flap was probably a result of a failure of the separated laminar boundary layer to reattach to the surface of the airfoil. The differences in lift curves for the airfoil section with a leading-edge flap at 0° deflection (fig. 7) and those for the basic airfoil section (fig. 2) were probably due to a slight surface discontinuity at the flap-skirt trailing edge which was not present on the basic airfoil.

Maximum lift.- Deflection of the leading-edge flap effectively added camber to the airfoil, and thereby delayed separation of the flow to greater angles of attack and increased the maximum lift coefficient. A summary of the maximum lift coefficients obtained for various deflections of the leading-edge flap is presented in figure 8. For deflections of the leading-edge flap from 0° to 10°, the maximum lift coefficient increased fairly rapidly; for deflections greater than 10° but less than 30°, the maximum lift coefficient remained nearly constant; and for deflections greater than 30°, the maximum lift coefficient decreased.

Lift, drag, and pitching moment.- The camber due to the deflection of the leading-edge flap caused an increase of the angle of attack for zero lift (fig. 7). Correspondingly, there was an increase in negative pitching-moment coefficient at zero lift and an increase in the angle of attack for minimum drag. The additional negative pitching moment due to deflection, which was quite large at small angles of attack, diminished with increasing angle of attack much in the same manner as that described for modifications 3 through 6.

Pressure distribution.- The chordwise variations of the pressure coefficient P for three values of lift coefficient with each of four leading-edge flap deflections are presented in figure 9. In the graphs of pressure distribution for the leading-edge flap, the locations of the pressure orifices on the deflected flap have been projected back to the original chord line. This permitted the pressure coefficients for both the flap and the circular-arc block to be plotted in their proper chordwise sequence starting from the leading edge and progressing toward the

trailing edge. With a leading-edge-flap deflection of 15°, two negative pressure peaks were established for the higher lift coefficients. For lift coefficients of 1.19 and 1.54, the peak at the leading edge predominated and undoubtedly was of sufficient magnitude to cause local laminar separation. Following reattachment of the flow to the surface of the airfoil, the turbulent boundary layer was then thinned by the increase in velocity associated with the second negative pressure peak and consequently had less tendency to separate when overcoming the pressure rise over the afterportion of the model. The over-all effect was to enable further increases of the angle of attack and consequently the lift of the model before the separated laminar boundary layer was unable to reattach to the surface. For lift coefficients approaching the maximum, the pressure distributions and the tuft observations indicated that the turbulent boundary layer was separated over the rear portion of the model with the leading-edge flap deflected 15°.

As the angle of deflection of the leading-edge flap was increased to 30°, the negative pressure peak near the leading edge was not present for the two lower values of lift coefficient (c_l = 0.61 and c_l = 1.17). Therefore, the flow probably remained laminar until the pressure began to rise behind the negative pressure peak associated with the circular-arc block. For angles of attack greater than 8°, however, the pressures near the leading edge decreased at a greater rate than those farther back on the leading-edge flap (fig. 10) so that, after an angle of attack of approximately 14° was reached, there existed the customary negative pressure peak near the leading edge. As a result, fully developed turbulent boundary-layer flow must be assumed to have occurred ahead of the second negative pressure peak for angles of attack greater than 14°. As the angle of attack for the maximum lift coefficient was approached, separation of flow began to appear near the trailing edge of the model. The existence of separation of the turbulent boundary layer as far forward as 80-percent chord prior to the stall was indicated by both the pressure distributions (fig. 9) and tufts.

For a 40° deflection of the leading-edge flap, the negative pressure peak near the leading edge was completely eliminated throughout the entire angle-of-attack range. For low and moderate angles of attack, tuft observations indicated that smooth flow was maintained to the negative pressure peak over the circular-arc block and that noticeably rougher flow took place in the region of pressure rise immediately following the peak. For angles of attack approaching those for maximum lift, only a slight amount of turbulent separation near the trailing edge was evident from the pressure distribution and tuft observations. The stall, resulting from the breakaway of flow over the circular-arc block, occurred before the customary negative pressure peak near the leading edge was established. To this cause must be attributed the decrease in the maximum lift coefficient for deflections greater than 30°. The flow separation resulting in the stall occurred instantaneously over the entire upper surface behind the circular-arc block but failed to disrupt the smooth character of the flow over the upper surface from the leading edge to the circular-arc block.

CONCLUSIONS

A wind-tunnel investigation of modifications to the leading-edge region of the NACA 63_1-012 airfoil section has shown the following results:

1. Modifications with greater-than-normal leading-edge radii combined with certain types of camber had a favorable effect on the maximum lift, but showed only slight improvements in the stalling characteristics. Modifications with greater-than-normal leading-edge radii and no camber and modifications incorporating a superposition of increased thickness showed little or no improvement over either the maximum lift or stalling characteristics of the basic airfoil section.

2. For the basic airfoil section with leading-edge flaps, the maximum lift coefficient increased fairly rapidly with flap deflections up to a deflection of 10°, remained nearly constant for the range of deflections from 10° to 30°, and decreased for deflections greater than 30°. The stalling characteristics throughout the range of leading-edge-flap deflections remained essentially those of the basic airfoil section.

Ames Aeronautical Laboratory,
National Advisory Committee for Aeronautics,
Moffett Field, Calif., Sept. 14, 1950.

REFERENCES

1. McCullough, George B., and Gault, Donald E.: An Experimental Investigation of an NACA 63_1-012 Airfoil Section with Leading-Edge Suction Slots. NACA TN 1683, 1948.

2. Liming, Roy A.: Practical Analytic Geometry with Applications to Aircraft. The MacMillan Company, N.Y., 1944.

3. Abbott, Ira H., von Doenhoff, Albert E., and Stivers, Louis S., Jr.: Summary of Airfoil Data. NACA Rep. 824, 1945.

4. Allen, H. Julian, and Vincenti, Walter G.: Wall Interference in a Two-Dimensional-Flow Wind Tunnel, with Consideration of the Effect of Compressibility. NACA Rep. 782, 1944.

5. Loftin, Laurence K., Jr., and Bursnall, William J.: The Effects of Variations in Reynolds Number Between 3.0×10^6 and 25.0×10^6 Upon the Aerodynamic Characteristics of a Number of NACA 6-Series Airfoil Sections. NACA TN 1773, 1948.

TABLE I.- COORDINATES FOR THE NACA 631-012 AIRFOIL SECTION

[Stations and ordinates given in percent of airfoil chord]

Station	Ordinate
0	0
.5	.985
.75	1.194
1.25	1.519
2.5	2.102
5	2.925
7.5	3.542
10	4.039
15	4.799
20	5.342
25	5.712
30	5.930
35	6.000
40	5.920
45	5.704
50	5.370
55	4.935
60	4.420
65	3.840
70	3.210
75	2.556
80	1.902
85	1.274
90	.707
95	.250
100	0
L.E. radius: 1.087-percent chord.	

TABLE II.- COORDINATES FOR THE VARIOUS LEADING-EDGE MODIFICATIONS
[Stations and ordinates given in percent of airfoil chord]

Leading-Edge Modification 1

Station	Ordinate
0	0
.5	1.125
.75	1.355
1.25	1.705
2.5	2.310
5	3.100
7.5	3.660
10	4.095
15	4.799
L.E. radius: 1.5-percent chord.	

Leading-Edge Modification 2

Station	Ordinate
0	0
.5	1.325
.75	1.575
1.25	1.936
2.5	2.525
5	3.238
7.5	3.727
10	4.124
15	4.799
L.E. radius: 2.0-percent chord.	

Leading-Edge Modification 3

Upper surface		Lower surface	
Station	Ordinate	Station	Ordinate
0	0	0	0
.5	.985	.5	-1.423
.75	1.194	.75	-1.730
1.25	1.519	1.25	-2.237
2.5	2.102	2.5	-3.118
5	2.925	5	-4.371
7.5	3.542	7.5	-4.993
10	4.039	10	-5.068
15	4.799	15	-4.799

Leading-Edge Modification 4

Upper surface		Lower surface	
Station	Ordinate	Station	Ordinate
0	0	0	0
.5	.985	.5	-1.823
.75	1.194	.75	-2.232
1.25	1.519	1.25	-2.915
2.5	2.102	2.5	-4.106
5	2.925	5	-5.799
7.5	3.542	7.5	-6.388
10	4.039	10	-6.173
15	4.799	15	-4.799

Leading-Edge Modification 5

Upper surface		Lower surface	
Station	Ordinate	Station	Ordinate
0	-0.919	0	-1.851
.103	-.575	.897	-3.103
.288	-.256	1.212	-3.268
.706	.246	1.794	-3.470
1.870	1.177	3.130	-3.713
4.394	2.473	5.606	-3.889
7.035	3.385	7.965	-4.011
9.743	4.038	10.257	-4.194
15.000	4.799	15.000	-4.799
L.E. radius: 2.0-percent chord. Center for L.E. radius: Sta., 1.945; Ordinate, -1.385.			

Leading-Edge Modification 6

Upper surface		Lower surface	
Station	Ordinate	Station	Ordinate
0	0.363	0	-3.243
.5	.985	.5	-3.889
.75	1.194	.75	-4.121
1.25	1.519	1.25	-4.471
2.5	2.102	2.5	-4.904
5	2.925	5	-5.080
7.5	3.542	7.5	-5.100
10	4.039	10	-5.040
15	4.799	15	-4.799
L.E. radius: 3.5-percent chord. Center for L.E. radius: Sta., 3.000; Ordinate, -1.440.			

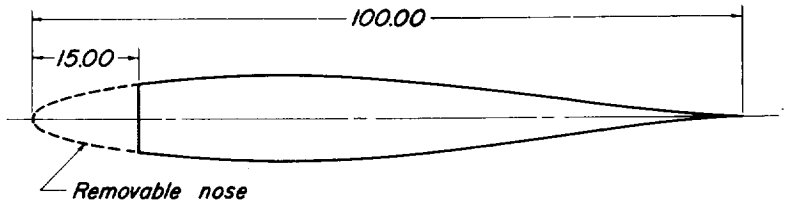

(a) Typical section through the model.

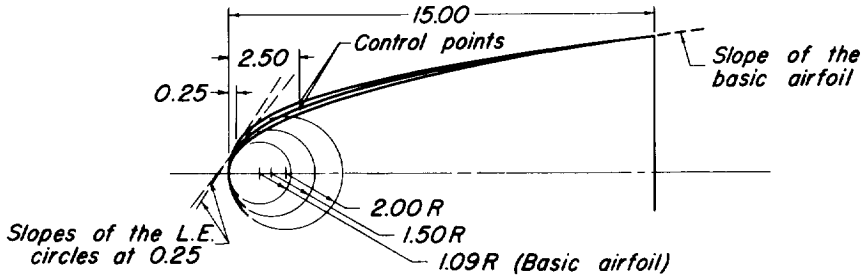

(b) Design details for modifications 1 & 2.

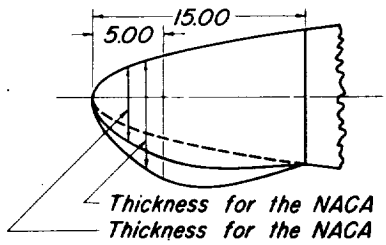

(c) Modifications 3 & 4.

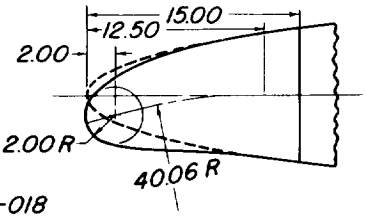

(d) Modification 5.

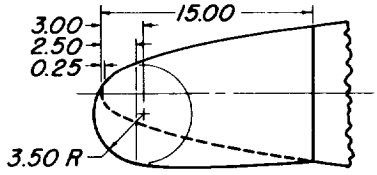

(e) Modification 6.

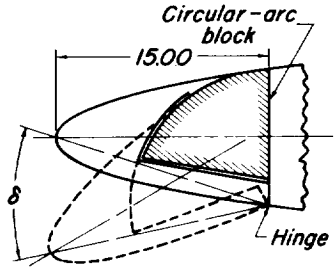

(f) Leading-edge flap.

Note: All dimensions in percent chord.

NACA

Figure 1.- Geometry of the model and the various leading-edge modifications.

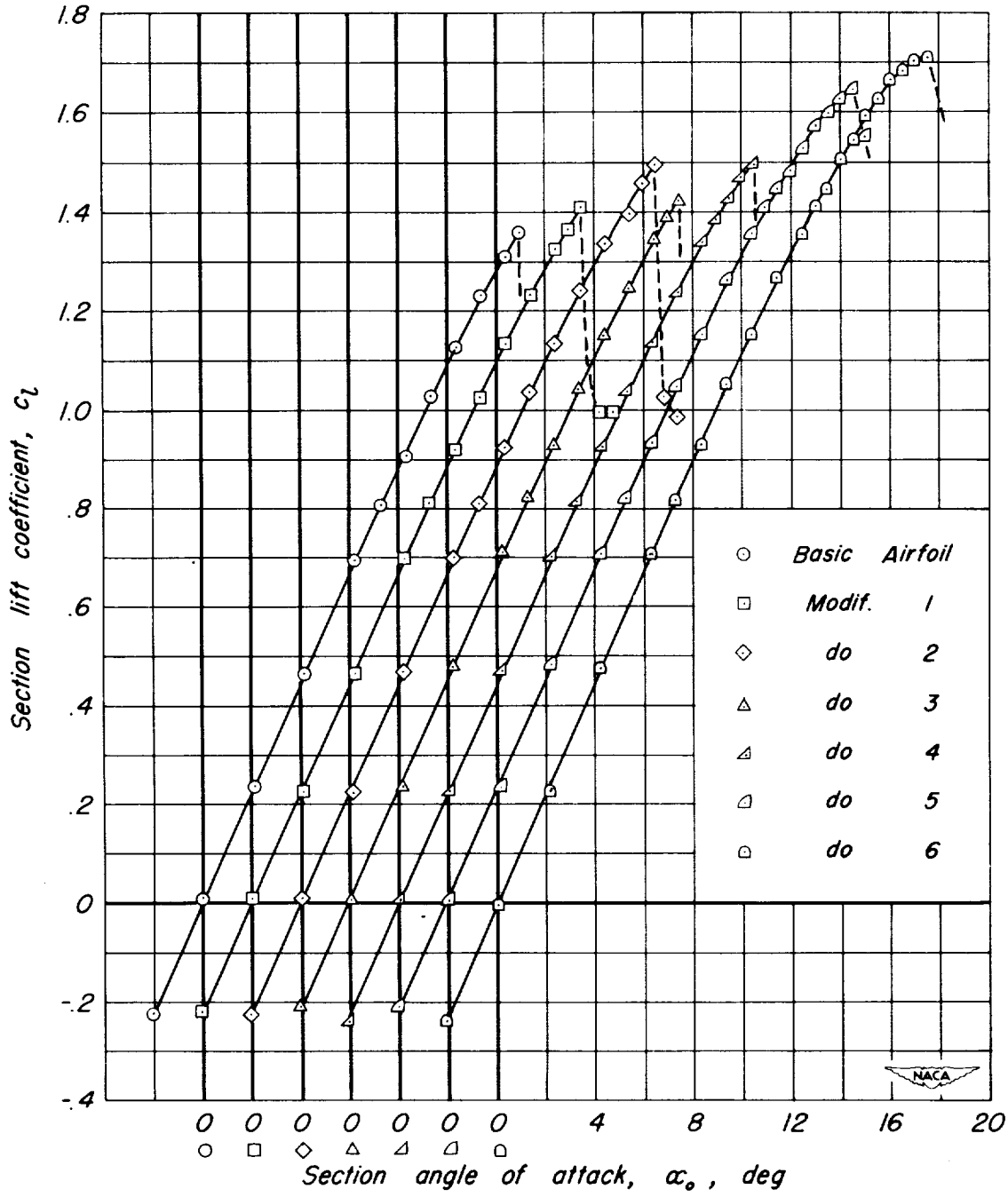

Figure 2.—Effects of the various fixed leading-edge modifications on the section lift characteristics of the model.

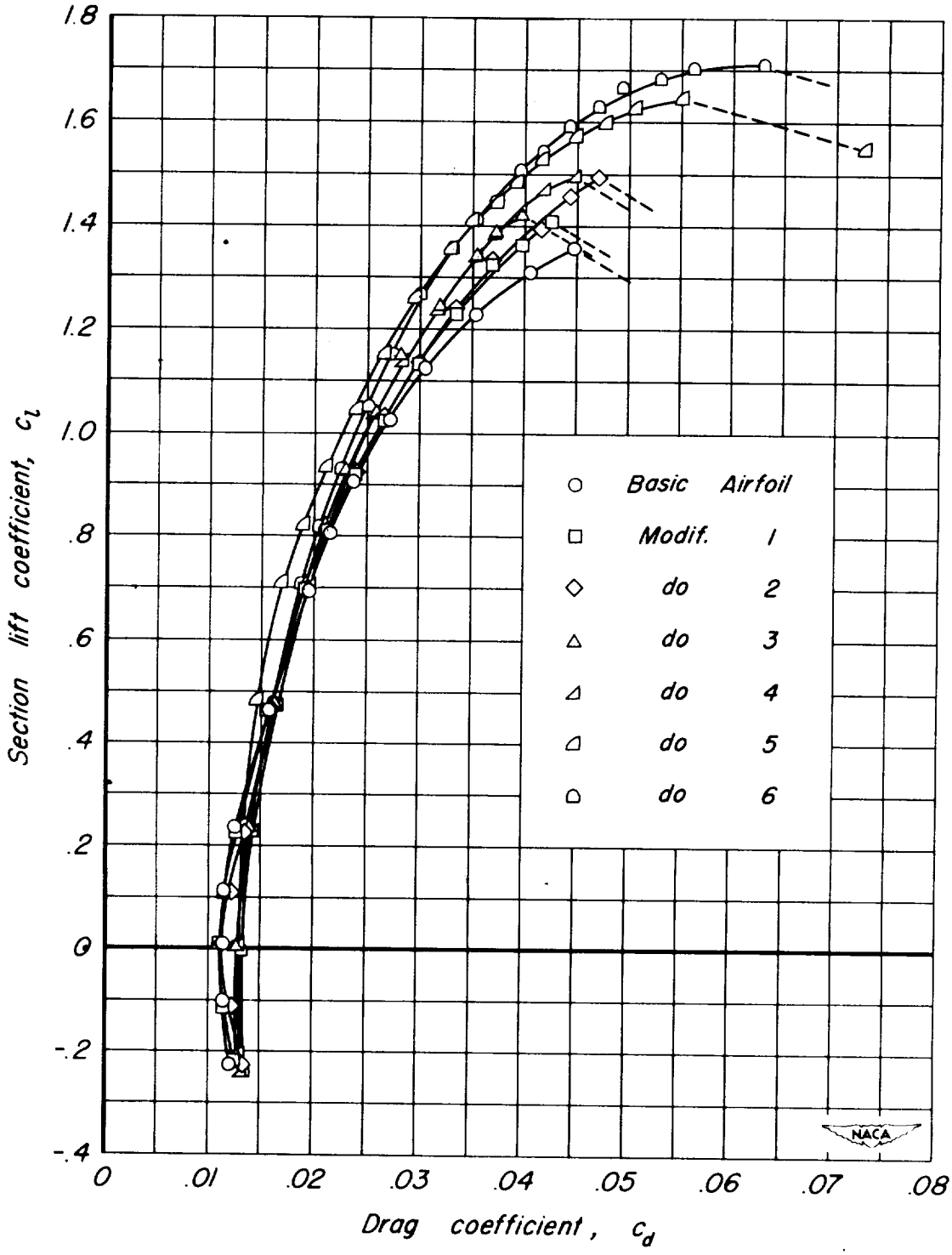

Figure 3.– Effects of the various fixed leading-edge modifications on the drag characteristics of the model.

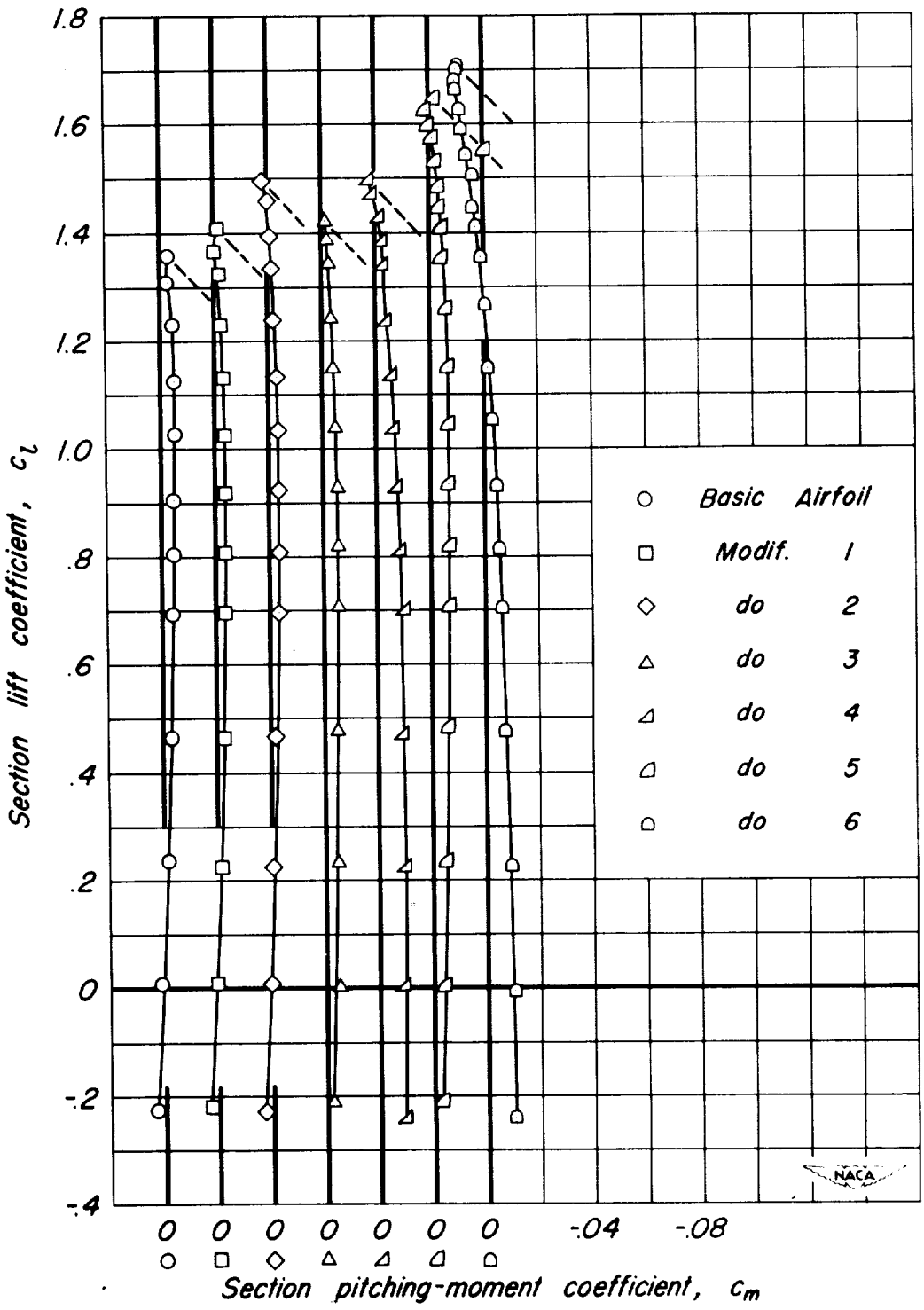

Figure 4.- Effects of the various fixed leading-edge modifications on the section pitching-moment characteristics of the model.

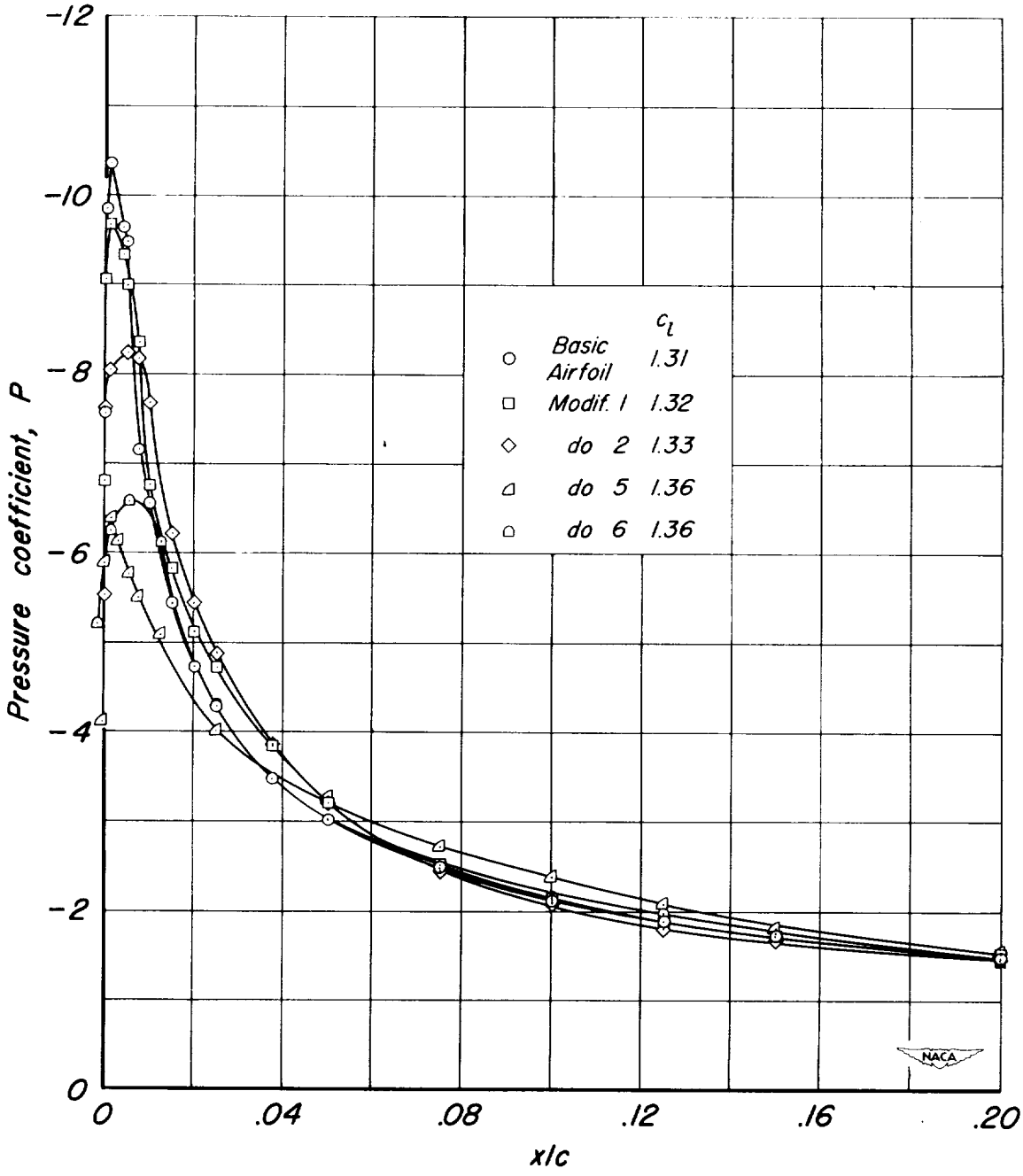

Figure 5.—Detailed upper-surface pressure distribution in the vicinity of the fixed leading-edge modifications.

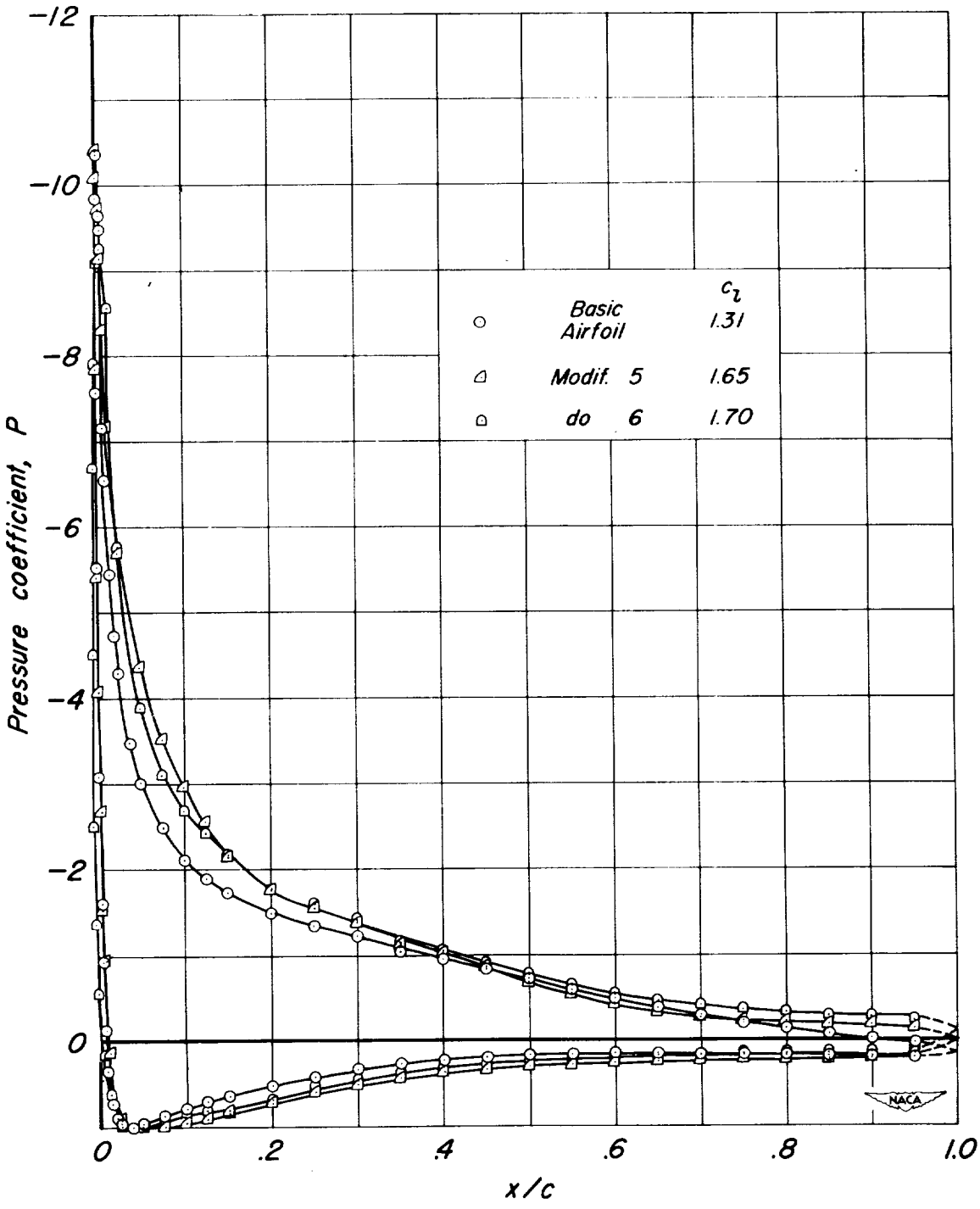

Figure 6.—Pressure distribution near maximum lift.

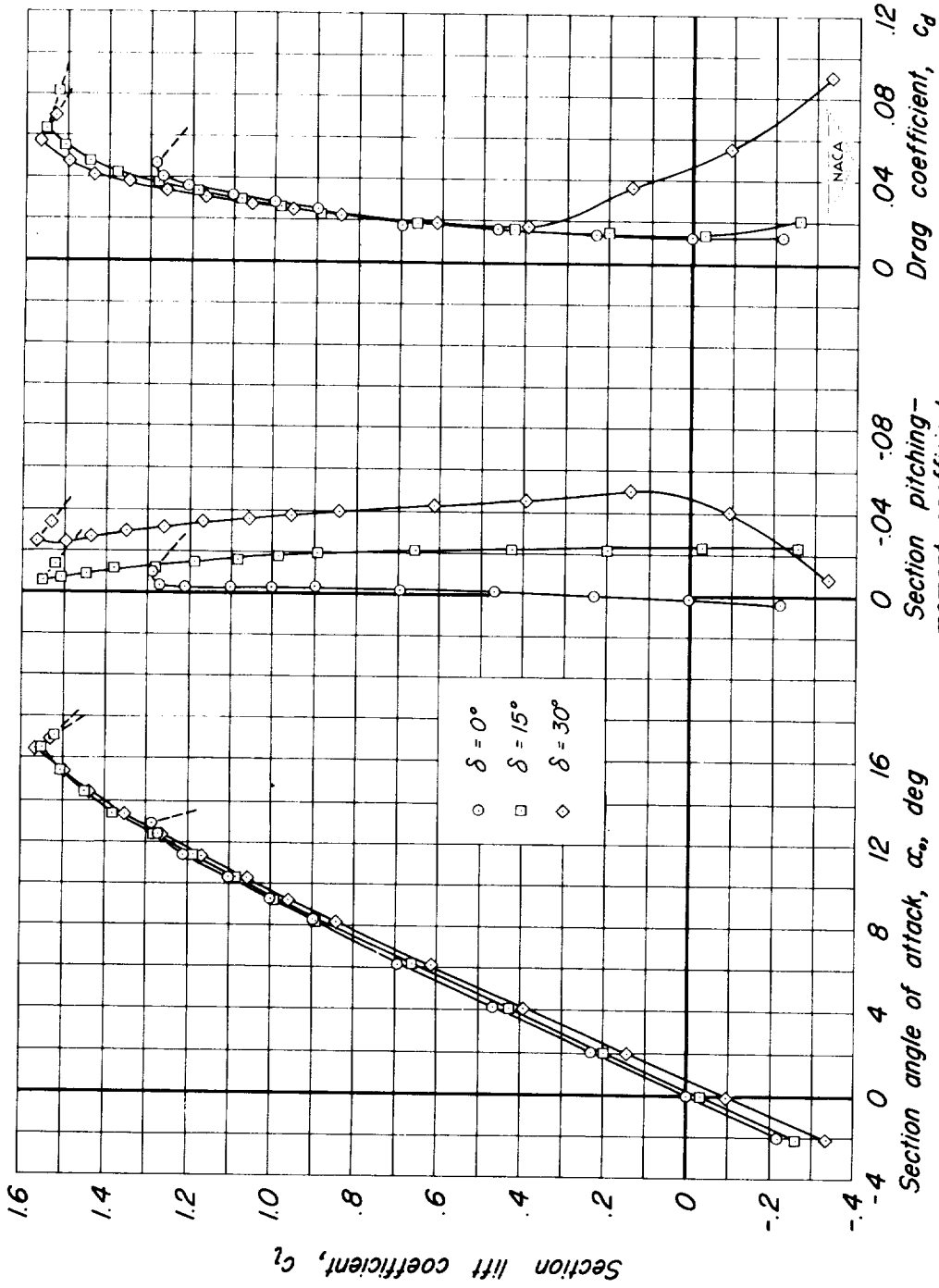

Figure 7.– The effect of leading-edge flap deflection on drag, section lift, and section pitching-moment characteristics of the model.

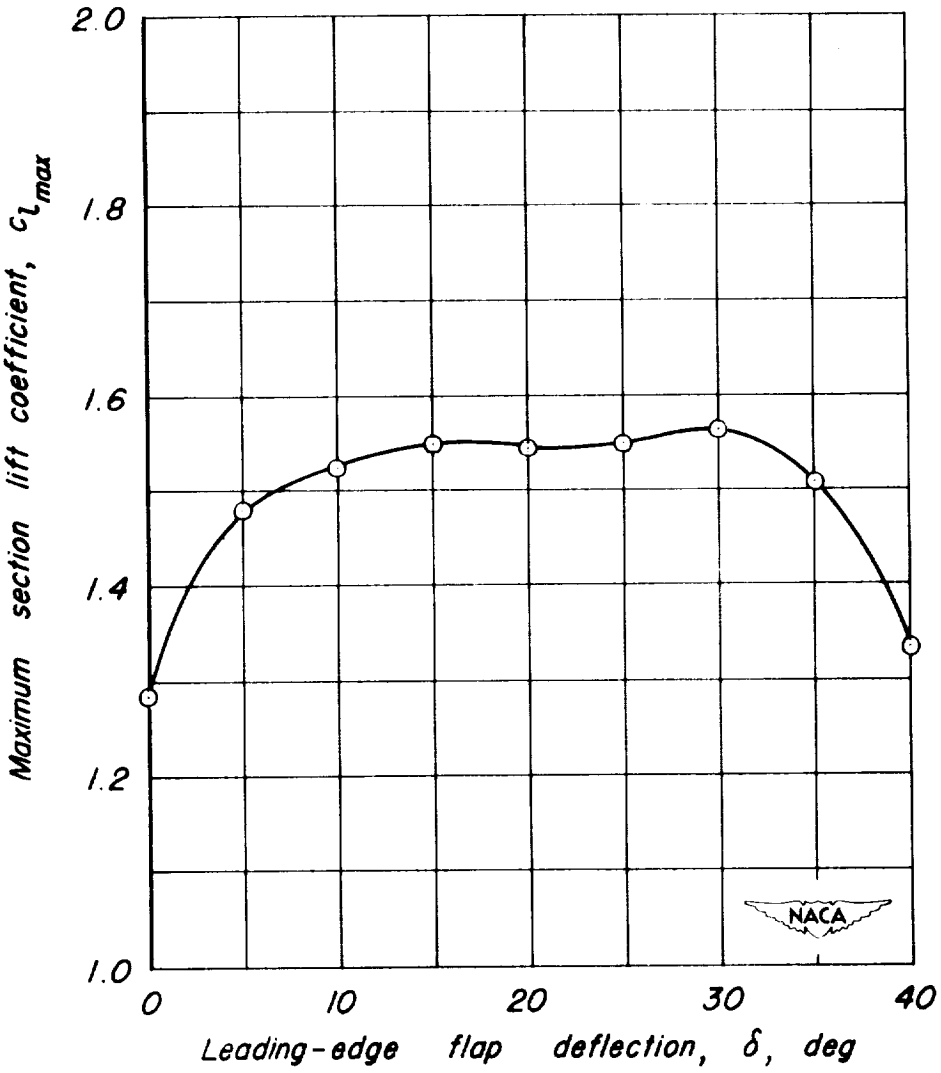

Figure 8.— The variation of maximum section lift coefficient with leading-edge flap deflection.

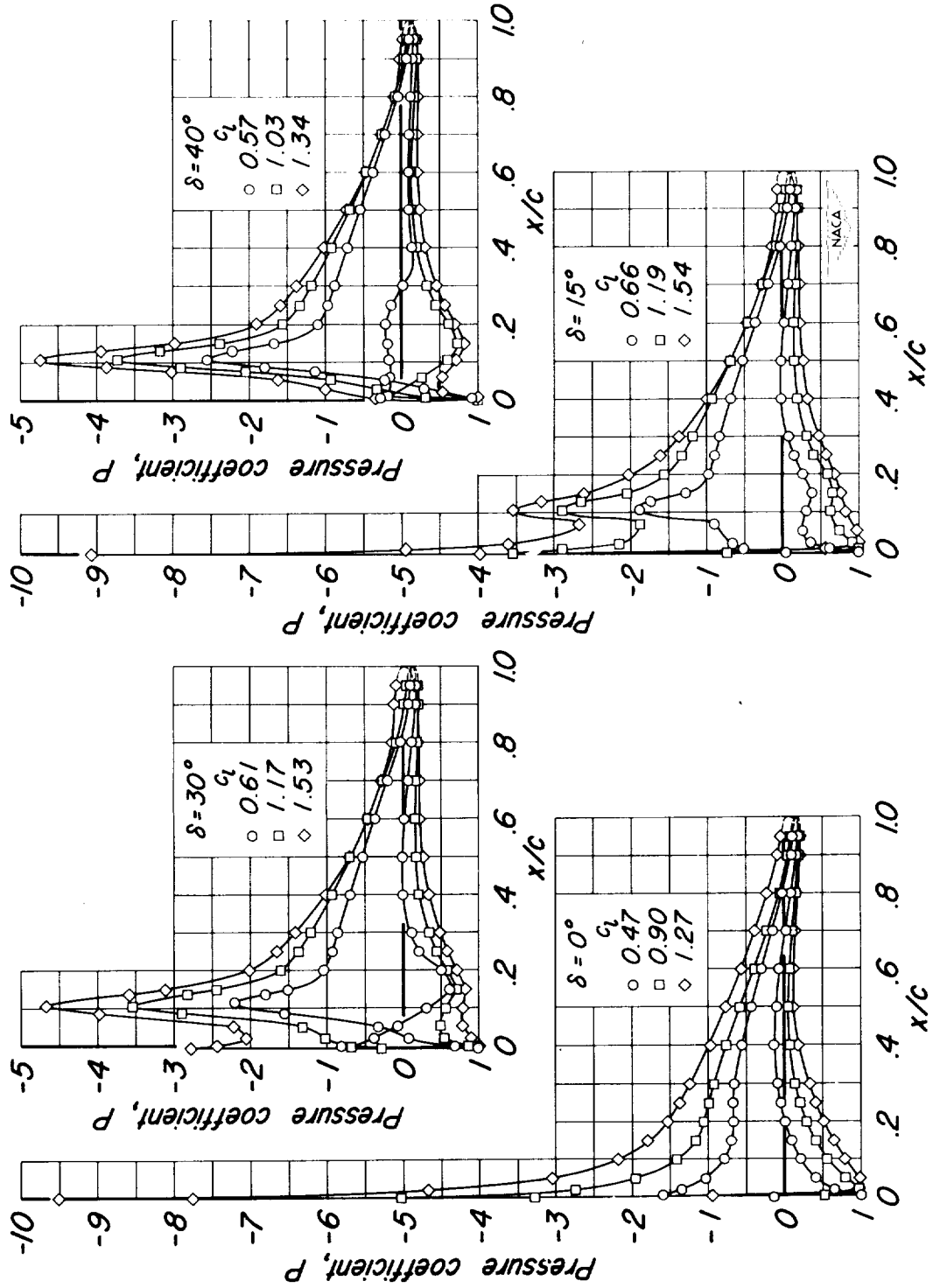

Figure 9.- Pressure distribution for the model with a leading-edge flap.

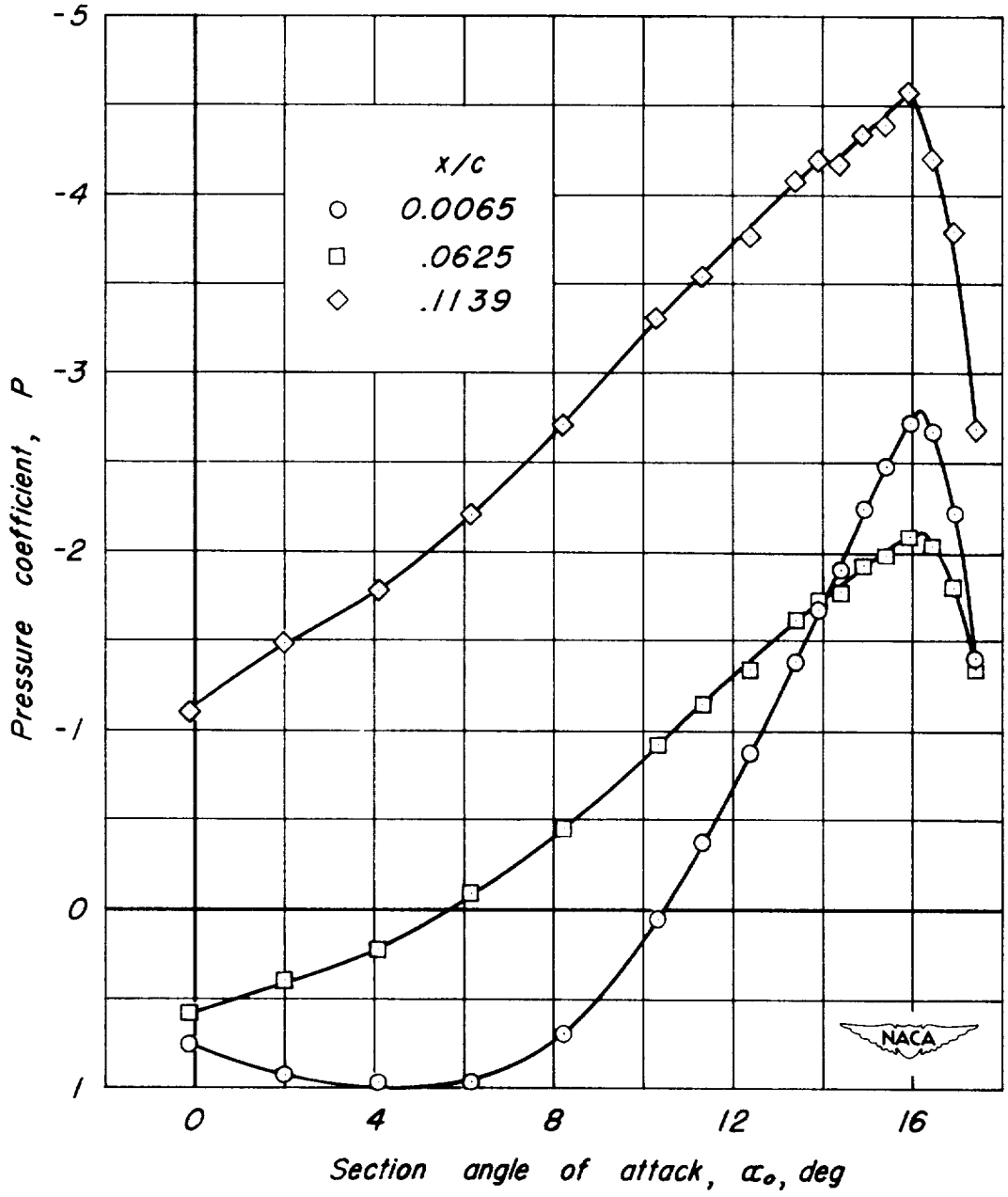

Figure 10.– The variation of pressure coefficient with angle of attack for the model with the leading-edge flap deflected 30°.

NACA-Langley - 11-27-50 - 1025